JCI insight

Multimodal integration of blood RNA and ctDNA reflects response to immunotherapy in metastatic urothelial cancer

Sandra van Wilpe, … , Pedro Romero, Niven Mehra

JCI Insight. 2025. https://doi.org/10.1172/jci.insight.186062.

Clinical Medicine In-Press Preview Immunology Oncology

BACKGROUND. Previously, we demonstrated that changes in circulating tumor DNA (ctDNA) are promising biomarkers for early response prediction (ERP) to immune checkpoint inhibitors (ICI) in metastatic urothelial cancer (mUC). In this study, we investigated the value of whole blood immunotranscriptomics for ERP-ICI and integrated both biomarkers into a multimodal model to boost accuracy.

METHODS. Blood samples of 93 patients were collected at baseline and after 2-6 weeks of ICI for ctDNA (N=88) and immunotranscriptome (N=79) analyses. ctDNA changes were dichotomized into increase or no increase, the latter including patients with undetectable ctDNA. For RNA model development, the cohort was split into a discovery (N=29), test (N=29) and validation set (N=21). Finally, RNA- and ctDNA-based predictions were integrated in a multimodal model. Clinical benefit (CB) was defined as progression-free survival beyond 6 months.

RESULTS. Sensitivity (SN) and specificity (SP) of ctDNA increase for predicting non-CB (N-CB) was 59% and 92%, respectively. Immunotranscriptome analysis revealed upregulation of T-cell activation, proliferation and interferon signalling during treatment in the CB group, contrary to N-CB patients. Based on these differences a 10-gene RNA model was generated, reaching a SN and SP of 73% and 79% […]

Multimodal integration of blood RNA and ctDNA reflects response to immunotherapy in metastatic urothelial cancer

Sandra van Wilpe[1*#], Davide Croci[2*#], Sara S. Fonseca Costa[2*], Iris B.A.W. te Paske[1], Sofie H. Tolmeijer[1], Jolique van Ipenburg[3], Leonie I. Kroeze[3], Simona Pavan[2], Sylvain Monnier-Benoit[2], Guido Coccia[2], Noushin Hadadi[2], Irma M. Oving[4], Tineke J. Smilde[5], Theo van Voorthuizen[6], Marieke Berends[7], Mira D. Franken[1], Marjolijn J.L. Ligtenberg[4], Sahar Hosseinian Ehrensberger[2], Laura Ciarloni[2], Pedro Romero[2], Niven Mehra[1]

1 Medical Oncology Department, Research Institute for Medical Innovation, Radboud University Medical Center, Nijmegen, The Netherlands

2 Novigenix SA, Epalinges, Switzerland

3 Department of Pathology, Research Institute for Medical Innovation, Radboud University Medical Center, Nijmegen, The Netherlands

4 Department of Medical Oncology, Ziekenhuisgroep Twente, Almelo, The Netherlands

5 Department of Medical Oncology, Jeroen Bosch Ziekenhuis, 's-Hertogenbosch, The Netherlands

6 Department of Medical Oncology, Rijnstate, Arnhem, The Netherlands.

7 Department of Medical Oncology, Canisius Wilhelmina Ziekenhuis, Nijmegen, The Netherlands

8 Department of Human Genetics, Research Institute for Medical Innovation, Radboud University Medical Center, Nijmegen, The Netherlands

* Equal contribution, the order was defined by random choice

Co-corresponding authors

Corresponding authors information:

Davide Croci, Route de la Corniche 3, Phenyl Building, 1066 Epalinges, Switzerland, phone: 0041 21 552 07 30, davide.croci@novigenix.com

Sandra van Wilpe, Radboud University Medical Center, 6525 GA Nijmegen, The Netherlands, phone: 0031 64 256 45 64, Sandra.vanWilpe@radboudumc.nl

Conflict of interest

D. Croci, S. S. Fonseca Costa, S. Pavan, P. Romero, G. Coccia and N. Hadadi are employees of Novigenix SA.

S. Hosseinian Ehrensberger, L. Ciarloni, S. Monnier-Benoit are cofounders and shareholders of Novigenix SA.

M. D. Franken has received honoraria from Servier (lecture), Ipsen (congress) and astellas (advisory board) (all paid to Radboud University Medical Center)

M. J. L. Ligtenberg participated in advisory boards of AstraZeneca, GlaxoSmithKline and Janssen Pharmaceuticals and was paid for educational activities by Roye congressen and Uitgeverij Jaap (all paid to Radboud University Medical Center)

N. Mehra has received research support from Astellas, Janssen, Pfizer, Roche and Sanofi Genzyme, and consultancy fees from Roche, MSD, BMS, Bayer, Astellas and Janssen (all paid to the Radboud University Medical Center).

The other co-authors declare no competing interests.

Abstract

Background: Previously, we demonstrated that changes in circulating tumor DNA (ctDNA) are promising biomarkers for early response prediction (ERP) to immune checkpoint inhibitors (ICI) in metastatic urothelial cancer (mUC). In this study, we investigated the value of whole blood immunotranscriptomics for ERP-ICI and integrated both biomarkers into a multimodal model to boost accuracy.

Methods: Blood samples of 93 patients were collected at baseline and after 2-6 weeks of ICI for ctDNA (N=88) and immunotranscriptome (N=79) analyses. ctDNA changes were dichotomized into increase or no increase, the latter including patients with undetectable ctDNA. For RNA model development, the cohort was split into a discovery (N=29), test (N=29) and validation set (N=21). Finally, RNA- and ctDNA-based predictions were integrated in a multimodal model. Clinical benefit (CB) was defined as progression-free survival beyond 6 months.

Results: Sensitivity (SN) and specificity (SP) of ctDNA increase for predicting non-CB (N-CB) was 59% and 92%, respectively. Immunotranscriptome analysis revealed upregulation of T-cell activation, proliferation and interferon signalling during treatment in the CB group, contrary to N-CB patients. Based on these differences a 10-gene RNA model was generated, reaching a SN and SP of 73% and 79% in the test and 67% and 67% in the validation set for predicting N-CB. Multimodal model integration led to superior performance with a SN and SP of 79% and 100% in the validation cohort.

Conclusion: The combination of whole blood immunotranscriptome and ctDNA in a multimodal model showed promise for ERP-ICI in mUC and accurately identified patients with N-CB.

Trial registration: 2016-3060, 2020-6778

Funding: Eurostars grant E! 114908 - PRECISE, Paul Speth Foundation (Bullseye project)

Introduction

In the last decade, immune checkpoint inhibitors (ICI) targeting programmed cell death 1 (PD-1) or its major ligand (PD-L1) have become one of the main treatment modalities for patients with irresectable or metastatic urothelial cancer (mUC). In 2017, pembrolizumab became the standard of care treatment for patients with mUC following progression on first-line platinum-based chemotherapy based on results of the KEYNOTE-045 (1). Since then, the use of ICI in patient with mUC has shifted to the first-line and maintenance setting. In 2021, maintenance therapy with avelumab became available for patients with a response or stable disease to first-line platinum-based chemotherapy (2). Very recently, the combination of pembrolizumab and antibody-drug conjugate enfortumab-vedotin (EV) became the new standard of care first-line treatment based on results of the EV-302. In this phase III clinical trial, pembrolizumab-EV prolonged median overall survival (mOS) from 16.1 to 31.5 months compared to platinum-based chemotherapy in the first-line setting (3,4). Another new first-line treatment option for patients who are eligible for cisplatin is the combination of nivolumab with cisplatin and gemcitabine, which has shown an OS advantage compared to cisplatin-based chemotherapy alone in the CheckMate 901 trial (5).

Although ICI-containing combination therapies have proven their superiority compared to first-line chemotherapy in unselected fit patients (3–5), it is anticipated that monotherapy ICI will continue to be an important treatment modality. First, ICI monotherapy will continue to play an important role in the treatment of frail or elderly patients with mUC because of the high toxicity associated with combination therapies. In addition, there might be a role for monotherapy ICI in biomarker-selected patients who are predicted to durably benefit from ICI monotherapy, regardless of frailty, to avert unnecessary toxicity and costs.

Responses to ICI in mUC are heterogeneous. Specifically, monotherapy ICI induces objective response in 20-25% of mUC patients receiving first- or second-line ICI and approximately 10% is still progression-free after 4 years (6,7). These latter patients might not derive extra benefit

from the addition of EV or chemotherapy. To personalize treatment decisions in mUC, there is a need for high precision biomarkers that can identify patients who benefit from ICI monotherapy. Several baseline tumor biomarkers, including tumor mutational burden (TMB), PD-L1 expression and tumor immune cell infiltration, have been associated with response to ICI in mUC (8–12). Although PD-L1 expression enriches for responders to first-line ICI in cisplatin-ineligible patients and is used to select patients for ICI over carboplatin-based chemotherapy, none of these standalone biomarkers are accurate enough to predict response to ICI.

In recent years, circulating tumor DNA (ctDNA) measurement has emerged as a method to monitor treatment response (13–15). The ctDNA level correlates well with tumor burden and can, therefore, be used as a non-invasive tool to monitor treatment response. We previously demonstrated that increases in ctDNA after 3-6 weeks are a promising biomarker for the early identification of disease progression to ICIs in mUC (15). However, ctDNA does not capture all host-related and tumor microenvironment-related factors that play a role in antitumor immunity. Multimodal biomarkers capturing both tumor and immune signals might improve biomarker accuracy.

In this study, we searched for on-treatment biomarkers that accurately identify patients without clinical benefit (N-CB), so that those with N-CB can be considered for other, more effective (combinatorial) therapies, while unwanted treatment discontinuation in patients with clinical benefit (CB) is avoided. We analyzed ctDNA and the peripheral blood immunotranscriptome in baseline and early on-treatment samples of mUC patients treated with ICI monotherapy. We show that early changes in the peripheral blood immunotranscriptome are associated with response to ICI and can be utilized to predict CB. Additionally, we demonstrate the synergy between ctDNA and whole blood RNA-sequencing data, by combining the two approaches in a multimodal model for early response prediction.

Results

Clinical characteristics of the ICI-treated mUC patient cohort

To longitudinally and non-invasively monitor response to ICI and to discover biomarkers predictive of CB, we collected blood liquid biopsies (LBx) from a total of 93 mUC patients treated with either pembrolizumab (N=72), nivolumab (N=7) or avelumab (N=14) (Figure 1A, Figure S1A and Table 1). Specifically, baseline (BL) blood LBx were collected before ICI therapy initiation, while on-treatment (OT) LBx were collected after cycle 1 or 2 (2-6 weeks). LBx samples were used for ctDNA and bulk whole blood RNA sequencing (RNA-seq) analysis (see material and methods section for details). We collected paired BL and OT ctDNA data for 88 patients and RNA-seq data for 79 patients, of whom 74 patients had both ctDNA and RNA data. Moreover, archival tumor tissue (FFPE) was used to determine PD-L1 CPS (N=62) and tumor mutational burden (TMB) (N=78) (Table 1). Of note, for RNA-seq analysis and modeling, patients were distributed in separate discovery, testing and validation cohorts for optimal data analysis (Figure S1A). Clinical endpoint was clinical benefit at 6 months, defined as radiological and clinical PFS at or beyond 6 months from treatment initiation. (Figure S1B). Out of the 93 patients included, 42 patients experienced clinical benefit (CB) and 51 did not (N-CB). Clinical characteristics are described in Table 1.

CtDNA profiling outperforms conventional tumor biomarkers for prediction of N-CB in ICI-treated mUC patients

High TMB and PD-L1 expression in the tumor have previously been associated with CB to ICI (16,17). We, therefore, assessed whether these two tumor biomarkers could help stratify the cohort into patients with or without CB (Figure 1, B and C). High PD-L1 expression was defined as a combined positive score (CPS) ≥10, in line with what is used in the clinic to select cisplatin-ineligible mUC patients for first-line ICI. There was a weak trend, but no significant association,

between CPS ≥10 and longer PFS (Figure 1B). High TMB, defined as a TMB ≥10 mutations per megabase, was significantly associated with improved PFS (Figure 1C), but low TMB had only 80% sensitivity and 43% specificity to predict N-CB. These results indicate that conventional tumor biomarkers only have partial ability to predict CB to ICI in mUC and that more accurate biomarkers are needed.

We previously demonstrated that decreases in ctDNA after 3-6 weeks show high specificity and moderate sensitivity for predicting CB to ICIs in a subset of patients of the presented mUC cohort (15). We expanded our previous cohort for the current analyses to a total of 88 patients. Patients were categorized into two groups based on their ctDNA dynamics. Patients with a ctDNA-increase or stable from BL to OT were predicted to have N-CB (N=32), while patients with a ctDNA-decrease from BL to OT (N=45) or undetectable ctDNA at both timepoints (N=11) were predicted to have CB. Patients with predicted CB had significantly longer PFS compared to those with predicted N-CB (Figure 1D). The ctDNA-based model showed 59% sensitivity and 92% specificity to detect N-CB patients (true positive cases) (Figure S1C). Additionally, a larger decrease in ctDNA level correlated with an extended time to progression (Figure S1D). Interestingly, ctDNA-based predictions partially correlated with PD-L1 CPS and TMB-based stratification (Figure S1E). Altogether, these data support the potential of ctDNA to predict N-CB, which outperforms the conventional tumor biomarkers PD-L1 and TMB.

Longitudinal immunotranscriptome analyses reveal biologically relevant changes in patients with CB to ICI

While early increases in ctDNA were highly specific for N-CB, only 59% of the patients with N-CB were identified with this approach, possibly related to the fact that ctDNA levels do not capture immune activity. We reasoned that the addition of a second approach capturing host immune response using LBx might improve biomarker accuracy compared to the ctDNA-only approach. We, therefore, decided to investigate if we could use the peripheral blood immunotranscriptome for early response prediction to ICI. To investigate this, patients were

distributed into independent discovery, testing and validation cohorts (Figure S1A). Specifically, the first cohort was used for biomarker discovery and model training, the second for independent model testing and optimization, and the third for final, blind, model validation.

For biomarker discovery, we first explored the longitudinal changes in gene expression in the CB patients in the discovery cohort (N=29). We performed differential gene expression analysis (DEA) comparing paired BL and OT samples of CB patients (longitudinal CB DEA) followed by pathway analysis of the differentially expressed genes (DEGs) (Figure S2A). Interestingly, among the over-representation analysis (ORA) of up-regulated processes at OT, we found several pathways related to cell cycle regulation and adaptive immune system signaling (including antigen presentation and interferon-γ signaling) (Figure 2A and S2B), while no significantly enriched pathways could be identified by analyzing the down-regulated DEGs. These results were confirmed by STRING network analysis of all DEGs which identified three highly interacting gene clusters related to T-cell activation, interferon-γ signaling and cell cycle regulation (Figure 2B, Figure 2C). The three gene clusters consisted mainly of genes that were up-regulated during treatment (Figure S2C) and included genes that have previously been associated with response to ICI, such as *PDCD1* (PD-1), Granzymes and *MKI67* (18–20). Moreover, STRING network analysis enabled the identification of biologically relevant genes down-regulated at OT, which included several myeloid cell-specific genes (*PVR, CD33, ENG, LY86, CD86, TNFRSF8, ASGR1*) belonging to STRING network cluster 1.

To identify the genes that discriminate CB and N-CB patients, we compared the longitudinal CB DEA DEGs to DEGs that are differentially expressed between BL and OT timepoints in N-CB patients (longitudinal N-CB DEA) and DEGs that were differentially expressed between OT samples of CB and N-CB patients (OT DEA) (Figure 2D and S2D). Interestingly, the longitudinal N-CB DEA (BL vs. OT timepoints) only revealed few DEGs (53 genes), of which only 7 genes were shared with the longitudinal CB DEA DEGs. By contrast, the OT DEA showed a larger overlap with the longitudinal CB DEA (49 genes), showing that these genes

not only are differentially regulated after treatment in the CB population, but also discriminate the CB and N-CB groups at OT timepoint. Functional analysis of the 49-gene intersect revealed pathways related to T-cell tolerance (Figure S2E). Altogether, the functional analysis of the longitudinal CB DEA highlighted multiple gene sets with the potential of discriminating the CB from the N-CB group.

We subsequently investigated whether the identified 49-gene set (Figure 2D) and the three STRING network clusters (Figure 2B) were able to separate the CB and N-CB patients. Specifically, we assessed the mean gene expression at OT in the CB and N-CB groups (Figure 2E and S2F) and patient clustering based on the gene expression at OT (Figure 2F and S2G). Interestingly, we found that the 49-gene set had a significant higher expression in the CB group and could separate the two populations by heatmap analysis (Figure 2E and 2F), while STRING cluster 1 to 3 gene sets could not achieve such separation (Figure S2F and S2G). These results indicated that immunotranscriptomic data from whole blood can detect biologically relevant signals of an early peripheral response to ICI. Moreover, the identified genes have potential to stratify the CB and N-CB populations.

Immunotranscriptome data and machine-learning (ML) approaches allow to develop robust models for early response prediction to ICI

To develop predictive models of CB to ICI, the DEGs identified in the longitudinal CB DEA of the discovery cohort were used as input to generate multiple models, using several iterations of biomarker subsets selection (Figure 3A and S1A) (see material and methods for details). Subsequently, the best performing immunotranscriptome model (RNA model) was selected based on predictions in the independent test cohort. This final RNA model, comprising 10 genes, was selected based on area under the curve (AUC) ranking of the receiver operating characteristics curve (ROC) for predicting CB to ICI and by ranking the difference in median PFS between the predicted CB and N-CB groups (Figure 3B-C and S3A-B). The RNA model

showed high performance in both independent test cohort (73% sensitivity at 79% specificity, AUC=0.84, N=29) and discovery cohort (92% sensitivity at 71% specificity, AUC=0.86, N=29). We then investigated the biological role of the 10 genes selected by ML-based feature reduction and used in the RNA model by mapping them to an attention map contextualizing the underlying biology (Figure 3D). We found that 8/10 genes (*PTTG1, RAD51, CLC, CD86, TOX, CEBPA, SMPD3, SCARF1*) could be contextualized to relevant biological functions of early response to ICI previously identified by ORA, such as T-cell activation and proliferation, while 2/10 (*PDXK* and a non-coding RNA) genes were not associated with previously identified pathways, but both belonged to the 49-gene set (Figure 2D). Interestingly, when using either the STRING gene clusters or the 49-gene set to develop predictive models, the performance in the test cohort was inferior to the 10-gene RNA model (Figure S3C). Also, the 10-gene panel did not show any overlap with a selection of literature-based tumor-derived signatures which have been shown to correlate with CB to ICI in other studies (Figure S3D) (21–23), although part of these genes was among the longitudinal DEA DEGs. Of note, models based on these literature-based signatures showed low performance in our cohorts (Figure S3E). Lastly, we validated the model performance in a small blind validation cohort (N=21). The RNA model achieved an AUC of 0.77 (67% sensitivity at 67% specificity, N=21) (Figure 3E) and there was a non-significant trend towards longer PFS in the predicted CB group (Figure 3F). To summarize, ML-based approaches for biomarker selection and modelling identified the most central RNA biomarkers in whole blood and showed high accuracy in the discovery and testing cohort for predicting CB.

Multimodal modelling with ctDNA and RNA-based biomarkers boosts model performance and leads to accurate prediction of N-CB in the independent validation cohort

Emerging evidence suggests that combining biomarkers from dissimilar sources can exponentially improve model performance (24,25). We, therefore, hypothesized that we could

improve predictions by integrating RNA- and ctDNA-based readouts in one model. When comparing the predictions of the standalone ctDNA- and RNA-based models in the test cohort (Figure 4A and Figure S4A), we found that models showed discordant predictions for a significant proportion of patients (12/27). We then reasoned that the fixed cutoffs used in the standalone models might influence wrong readout occurrence. Indeed, false positive and false negative cases of both the RNA and the ctDNA model had a prediction probability and, respectively, a ctDNA ratio close to the cutoff values (Figure S4B and C). Therefore, we developed a multimodal model in the test cohort where the final prediction was based on a cutoff range of combined ctDNA ratio and RNA-based prediction probability (see material and methods section for details). The multimodal model was then validated in the independent validation cohort. The multimodal model showed superior performance compared to the standalone approaches (Figure 4B), reaching 71% sensitivity at 100% specificity in the test cohort, and 79% sensitivity at 100% specificity in the independent blinded validation cohort. Consequently, the multimodal approach allowed for a superior stratification of the predicted CB and N-CB groups (Figure 4C-E). Thus, this multimodal analysis appears a promising tool for early response prediction to ICI.

Discussion

In this study, we performed ctDNA and whole blood immunotranscriptome analyses to identify biomarkers for early response prediction to first- and second-line and maintenance ICI in patients with mUC. We confirmed that early changes in ctDNA levels are associated with CB to ICI, with early increases in ctDNA levels being highly specific for N-CB. We hypothesized that peripheral blood immunotranscriptome analyses might be a valuable complementary approach to ctDNA and indeed found it to be a promising tool for early response monitoring in mUC. In patients with CB to ICI, pathways related to cell cycle regulation, T cell activation, antigen presentation and interferon-gamma signaling were upregulated already three weeks after the first anti-PD-(L)1 infusion. These changes were specific for patients with CB, which enabled the generation of a 10-gene model to predict CB based on whole blood immunotranscriptome data with high accuracy. A multimodal model incorporating both ctDNA and immunotranscriptome-predictions showed superior performance compared to both standalone predictions and conventional biomarkers (PD-L1 and TMB) and demonstrated a sensitivity of 79% and specificity of 100% for prediction of N-CB in an independent blinded validation cohort.

There are currently no clinically applicable biomarkers to identify patients that derive benefit from ICI. In current practice, ICI are usually continued for at least 12 weeks, at which point the first radiological response evaluation is performed. Clinically stable patients with suspected progression after the first scan according to iRECIST may continue treatment to avert treatment discontinuation in patients with pseudo-progression or a delayed response (26). Early response biomarkers would facilitate the early identification of patients without CB, thereby limiting unnecessary costs and toxicities. Additionally, the use of early response biomarkers may improve clinical outcomes by facilitating an early treatment switch or treatment intensification in patients that do not benefit from ICI monotherapy. Early on-treatment biomarkers would, therefore, be of great value in the clinic.

In this study, we observed that changes in ctDNA levels during ICI treatment are associated with clinical outcome. Others have described comparable associations between ctDNA kinetics and clinical outcome following ICI in multiple cancer types, but the optimal cutoff remains to be elucidated (27–33). Raja et al. showed a relation between increases in ctDNA fraction and disease progression in 28 mUC patients treated with ICI, similar to our data (34). Powles et al. recently presented ctDNA data of the phase III KEYNOTE-361 trial. Changes in ctDNA fraction during the first 3 weeks of pembrolizumab were smaller than during chemotherapy, but showed a stronger association with clinical outcomes. Additionally, patients with a large reduction in ctDNA after 3 weeks, defined as a reduction above median across both treatment groups, demonstrated higher objective response rates and better OS (28). In our study, we chose to split the cohort into patients with or without a ctDNA increase in order to detect patients with N-CB with high certainty. This way clinicians and patients could confidently decide on an early treatment switch or intensification without risking halting an effective treatment. Nevertheless, when using another cutoff it might also be possible to use ctDNA to detect long-term responders with high specificity, as observed in our dataset (Figure S1D).

To improve early response prediction based on ctDNA-data alone, we reasoned that the addition of a second approach that reflects immunological activity might improve our predictions. To enable non-invasive monitoring of peripheral immune activity, we investigated the potential of whole blood immunotranscriptome analyses for the early identification of response to ICI in mUC and were able to generate a 10-gene model to predict CB based on peripheral blood immunotranscriptome data with high accuracy.

Although our immunotranscriptome analyses were performed on bulk RNA-sequencing data, we found several biologically relevant pathways to be upregulated during the first weeks of therapy in patients with CB to ICI, including pathways involved in cell cycle regulation, T cell activation and antigen presentation and interferon-gamma signaling, confirming that whole blood immunotranscriptome data is a reliable source to detect ICI-related changes in

peripheral blood. Interestingly, we found some immune-related genes that have previously been associated to response to ICI in other studies using tumor biopsies (21–23), highlighting the capability of our LBx approach to detect parallel gene dysregulation in the blood. Of note, while several studies have investigated the relationship between baseline tissue transcriptome and response to ICIs, studies using peripheral blood transcriptome data are scarce. Interestingly, a recent study by Richard et al. showed that genes associated with immune cell activation are overexpressed in baseline samples of mUC patients responding to durvalumab, whereas patients with progressive disease overexpressed genes of immune cell inhibition (35). These authors, however, did not study on-treatment changes in whole blood RNA. While data on early changes in peripheral blood transcriptome in patients treated with ICI are lacking, our findings are in line with previous flow cytometry and single cell sequencing studies, demonstrating proliferation of (activated) T cells during the early phase of ICI therapy in patients that benefit from ICI (18,19,36).

Whereas longitudinal ctDNA dynamics reflect changes in tumor burden and biological activity, whole-blood immunotranscriptome dynamics reflect early, systemic adaptations in immune-cell activity and proliferation. We, therefore, hypothesized that a multimodal model capturing both ctDNA and whole blood immunotranscriptome predictions might outperform the standalone approaches. Our multimodal model indeed showed superior performance compared to the standalone approaches. While the ctDNA standalone approach had a sensitivity and specificity of 64% and 100% and the RNA standalone approach 67% and 67% in the independent validation cohort, the multimodal model reached 79% sensitivity and 100% specificity.

While our multimodal model will need further validation before it can be implemented in the clinic, our model shows promise as non-invasive biomarker test for the early detection of N-CB to ICIs. The high specificity will allow clinicians and patients to confidently decide on an early treatment switch without risking halting an effective treatment. While it would be acceptable to miss some patients with N-CB, we should aim to further optimize the sensitivity

of our test in subsequent studies. One possibility to optimize test performance is the incorporation of a second, early, on-treatment sample. Our previous ctDNA study (15) analyzed 20 patients with both 3-week and 6-week samples. Two patients with N-CB showed a ctDNA decrease at 3 weeks, but an increase at 6 weeks. On the other hand, one patient with CB showed a rise in ctDNA at 3 weeks and then a decrease compared to the 3-week timepoint at 6 weeks. These data suggest that more insight into early dynamics of ctDNA might further improve performance of our test. Another way to improve our test is by incorporating additional mUC-associated genes in the ctDNA panel (e.g. KMT2D and KDM6A) (15). It is possible that a few patients with undetectable ctDNA in our study had false-negative results and were incorrectly categorized, negatively influencing the accuracy of our ctDNA prediction. Further optimization of our ctDNA panel could limit the number of patients with false negative ctDNA testing.

Our multimodal model based on whole blood immunotranscriptome and ctDNA data shows promise as a non-invasive blood-based biomarker test for early identification of N-CB to ICIs in mUC. Interestingly, the model obtained accurate predictions in both patients treated with first- or second line ICI as well as in patients treated with avelumab maintenance, emphasizing the robustness of the test. Yet this study also has some limitations. First, the study cohorts were small, particularly the number of patients with paired ctDNA and RNA data in the independent validation cohort (N=19). Validation of our multimodal model in larger cohorts is needed before it can be implemented in the clinic. Another limitation is that the use of ICI monotherapy may decline in the near future due to changes in the treatment landscape of mUC. Nevertheless, we anticipate that monotherapy ICI will continue to be an important treatment modality for frail or elderly patients with mUC because of the high toxicity associated with combination therapies. Additionally, it would be very interesting to test if our multimodal biomarker approach can be used in the first line setting to limit the use of intensive combination therapies to patients that do not durably benefit from monotherapy ICIs. For instance, patients could receive pembrolizumab monotherapy in the first line mUC setting and could then

escalate to pembrolizumab-EV if the multimodal test predicts that the patient is not responding. This strategy may particularly be of interest in patient subgroups that derive increased benefit of ICI monotherapy, such as those with lower ctDNA fractions or those with lymph node-only disease (28,37).

While the current study tested the predictive value of early ctDNA and whole blood RNA kinetics in patients receiving ICI monotherapy, it would also be of interest to test these biomarkers in patients receiving ICI-containing combination strategies, such as EV or cisplatin-gemcitabine. Not all patients derive benefit from addition of ICI, and response patterns from longitudinal assessment might distinguish those that derive benefit from combination therapy, or EV or ICI alone.

In conclusion, whole blood immunotranscriptomics provides a promising tool for early response prediction to ICI in mUC, particularly when used in a multimodal model together with changes in ctDNA levels. Results of our multimodal analyses should be validated in clinical trials to confirm that the test can be used to improve clinical outcomes of mUC patients.

Material and methods

Sex as a biological variable

Both female and male patients were included. In this study, sex was not considered as a biological variable.

Patients

This Dutch, multicenter study included 93 patients with mUC who were treated with anti-PD-(L)1 between 2017 and 2023. Patients were treated with nivolumab or pembrolizumab in the first- or second-line mUC setting or with maintenance avelumab following response or stable disease to platinum-based chemotherapy. Patients with measurable disease were evaluated according to RECIST1.1 (38). Clinical endpoint was clinical benefit (CB) at 6 months, defined as radiological and clinical progression-free survival (PFS) at 6 months, which was previously demonstrated to show a better correlation with overall survival in mUC than objective response(39). Patient demographic is reported in table 1.

Blood Collection and Processing

Blood was drawn prior to the first three cycles of anti-PD-(L)1 therapy (i.e., at 0, 2 and 4 weeks for nivolumab and avelumab and at 0, 3 and 6 weeks for pembrolizumab). At these timepoints, a complete blood cell count was performed as part of routine clinical care. In addition, blood was collected in a PAXgene Blood RNA tube for whole blood RNA analyses (BD Biosciences, San Jose, CA, USA) and in three 10 mL EDTA or cell-free DNA (cfDNA) collection tubes (Roche) for ctDNA analyses. PAXgene tubes were stored at −80°C until RNA purification. EDTA and cfDNA tubes were processed as previously described (15). The baseline sample and the earliest on-treatment sample available were used for analyses.

TMB and PD-L1

Tumor tissue for molecular analysis and PD-L1 staining was obtained from diagnostic biopsies obtained in routine clinical practice. The PD-L1 staining was performed on formalin-fixed paraffin-embedded (FFPE) tissue sections using antibodies against 22C3 (PharmaDx kit, DAKO Agilent, #GE006) or E1L3N (Cell Signalling, #13684S). A combined positivity score (CPS) was calculated by dividing the number of stained cells expressing PD-L1 (tumor cells, tumor-associated lymphocytes and macrophages) by the total number of viable tumor cells, multiplied by 100, taking into account at least 200 viable tumor cells, not adjacent to necrotic areas. A CPS≥10 was considered positive.

Tumor sequencing data were generated utilizing different sequencing platforms: whole genome sequencing (WGS), whole exome sequencing (WES), TruSight Oncology 500 (TSO500), Foundation Medicine T7 assay (CLIA: 22D2027531), single molecule Molecular Inversion Probe panel (PATHv3D) and/or the ctDNA_NGSv1 targeted sequencing panel (15). WGS, WES and TSO500 data were used to determine non-synonymous tumor mutational burden (nsTMB). A nsTMB≥10 mutations per megabase was considered high.

ctDNA

ctDNA analyses were performed in 88 patients, of which 53 patients were included in a prior publication (15). Only patients with paired baseline and on-treatment samples who were evaluable for the clinical endpoint were included in the current analyses.

ctDNA workup and downstream analysis were performed as previously described (15). In short, cell-free DNA (cfDNA) was isolated from blood plasma (median 5.6 mL, IQR 5 mL - 8 mL) using the QIAamp Circulating Nucleic Acid kit (Qiagen). White blood cell (WBC) DNA was isolated using a QIAamp DNA Mini Kit (Qiagen). A maximum of 50 ng cfDNA ng (median 50 ng, IQR 37 ng - 50 ng) and 50-80 ng of mechanically sheared WBC DNA were used for targeted sequencing using an in-house developed and validated 117 kb targeted sequencing panel (NEN-EN-ISO 15189+C11:2015) (15). Libraries were generated using the TWIST Library Preparation Kit (TWIST Biosciences) in combination with xGen dual index unique molecular identifiers (UMI) adapters (Integrated DNA Technologies) or TWIST UMI adapters (TWIST

Biosciences). Libraries were paired-end sequenced on a NovaSeq6000 platform (Illumina). Reads were mapped to hg19 and deduplicated using the read-specific UMI information (Fgbio). Unique reads that not met fgbio quality parameters and/or based on <2 UMI reads (singletons) were only kept for variant detection in *TERT* protomer region and copy number variant (CNV) detection.

Somatic variants were called using Genomic Analysis Toolkit (GATK) Mutect2 (version 4.1.5.0) based on previously described filter criteria (15). Variants with at least 5 supporting variant reads and >0.1% variant allele fraction (VAF) were selected for downstream analysis. Additionally, patient-specific cfDNA variants and, if available, tumor variants (evaluation of nonsynonymous tumor variants with a minimal read depth of 10, N=59 pts), were evaluated in the patient-matched BL and OT cfDNA sequencing data. For this dependent calling, the variant in the matched BL or OT sample had to be supported by at least 3 variant reads, the VAF signal had to be at least 20x higher than the average VAF of 22 control cfDNA samples and at least three times higher than the patient-matched WBC sample for that specific nucleotide change (if available).

CNV detection was performed as previously described using both the relative coverage and the median allele fraction (MAF) divergence from heterozygosity. Copy number loss was defined as relative coverage ≤ −0.3 or relative coverage ≤ −0.1 and MAF ≥ 0.6. Copy number gain was defined as a relative coverage ≥ 0.3 or ≥ 0.1 and MAF ≥ 0.6.

CtDNA fraction was determined by using the somatic mutation with highest VAF in a non-amplified region corrected for loss of heterozygosity (LOH) or using the MAF deviation from heterozygosity of germline single nucleotide polymorphisms (SNPs) in genes with a single-copy loss (15,40). CtDNA fractions were converted to ctDNA copies per mL plasma (total cfDNA concentration multiplied by 303). To incorporate technical uncertainty and biological variability of ctDNA levels, lower and higher limits were estimated as previously described (15). On-treatment changes were dichotomized into increase versus no increase, based on changes in ctDNA copies/mL. Patients with an increase were predicted to not have CB (N-CB), whereas patients without an increase during treatment were predicted to have CB. Patients with

undetectable ctDNA in both the baseline and on-treatment sample were categorized as no increase/predicted-CB since low baseline ctDNA levels are considered a prognostically favorable sign (28). CtDNA-based specificity and sensitivity was calculated for the full ctDNA cohort.

Whole Blood RNA Sequencing

Whole blood RNA sequencing was performed in 79 patients with paired samples. Additionally, 2 patients with on-treatment samples only were used for differential gene expression analysis (DEA). Total RNA was extracted from whole blood using the PAXgene blood miRNA kit (Qiagen, Venlo, Netherlands). RNA quantity was determined using Qubit (Thermo Fisher Scientific, Waltham, MA, USA). RNA quality was assessed on a Tapestation 4,200 (Agilent Technologies, Santa Clara, CA, USA). Per sample, at least 200 ng of total RNA was used for library preparation. RNA samples were treated for globin RNA depletion with the QIAseq FastSelect RNA Removal kit (Qiagen, Venlo, Netherlands). Library preparation was performed after isolation of poly-A RNA by means of NEBNext poly(A) mRNA magnetic isolation module and then, setup of directional RNA libraries by means of NEBNext Ultra II directional RNA library prep kit in combination with NEBNext multiplex oligos for Illumina Set 1, Set 2 and Set 3 was performed (NEB, Ipswich, MA, USA). Library quality control was done by using Dual AmpureXP cleanup for complete adapter dimer removal, and a verification of adapter dimer removal with TapeStation 4,200 (Agilent Technologies, Santa Clara, CA, USA).

All Libraries were pooled by equal volume and a test sequencing run was done on iSeq100 (Illumina, San Diego, CA, USA) to determine content of each library and adjust the final pool. Sequencing was performed on Illumina NovaSeq6000, 3 lanes of S4 flow cell, Paired-End 150 configuration with an expected output of 800Gb per lane or ca. 2,600M PE reads per lane (Illumina, Sain Diego, CA, USA). A minimum of 30M PE150 reads were required per sample.

The FastQ files with paired-end reads were used as input for gene expression analysis on the LITOSeek® platform (Novigenix SA, Epalinges, Switzerland). Of note, whole blood RNA sequencing data of patients in the discovery cohort has been previously published (20).

Samples have been re-sequenced and re-analyzed for this paper after optimization of the analyses pipeline.

Data processing and Quality Check

Sequence data quality was evaluated using FastQC (version 0.11.9) combined with MultiQC (version 1.11). Cutadapt (3.4) was used to find and remove adapter sequences, primers, poly-A tails and other types of unwanted sequence from high-throughput sequencing. Reads were aligned to the Human genome assembly (GRCh38) along with its corresponding annotation from Ensembl database using the release 107. The pseudo-alignment and quantification of transcript abundance of the RNA-Seq reads was done using Salmon (version 1.5.2) with default parameters. All samples were used for downstream analysis.

Data transformation and exploratory analysis

Normalization for gene length, Transcripts Per Million (TPM) values, was conducted as a step downstream in our analysis. Gene pseudo-counts from Salmon were imported into the R statistical computing environment (version 4.2.1) and subsequently filtered by excluding genes with less than 1 count per million (CPM) across all samples and with a coefficient of variance (cv) of 100, using the filtered.data function within the NOISeq R package (version 2.40.0). Following the initial gene data treatment, forward normalization was performed employing the variance-stabilizing transformation using the vst function, which is a feature of the DeSeq2 R package (version 1.36.0). Primary focus for exploratory data analysis centered on the vst-transformed values and the selected subset of genes from NOISeq. Principal Component Analysis (PCA) and scatter plots were applied to visualize the similarities and differences among samples.

Differential gene expression and multivariate analysis

Comprehensive analysis of differential gene expression was performed using proprietary algorithms and curation of the differentially expressed genes (DEGs). Three DEAs were

performed: the first compared the on-treatment (OT) samples of patients with CB with their paired baseline (BL) samples, the second compared the OT and BL samples of patients with N-CB and the third compared the OT samples of patients with CB versus patients with N-CB. Functional and network analyses of the DEGs were realized with STRING (version 12.0) and Cluster-Profiler (version 4.6.2) to perform over-representation analysis (ORA), which allowed to identify central biological pathways and biomarkers of response. STRING clusters were defined by MCL clustering (inflation parameter=3) on the STRING online platform by inputting the longitudinal DEA CB DEGs. Significantly enriched ORA pathways were defined by an adjusted p-value≤0.05 (Benjamini-Hochberg method). Additionally, the DEGs attributed to any enriched terms from the ORA results output were extrapolated, enabling identification of the functionally relevant genes among all DEGs. Basic plots were performed with RStudio (version 4.2.1) and the correspondent R packages ggplot2 (version 3.5.0), UpSetR (version1.4.0). Heatmaps were generated with ComplexHeatmap (version 2.14.0), ROCR (version 1.0-11) was used to plot ROC curves, survminer (version 0.4.9) and survival (version 3.5-8) were used to generate Kaplan Meier curves for PFS.

Modeling

To develop predictive models of CB to ICI, the DEGs identified in the longitudinal CB DEA of the discovery cohort were used as input to generate multiple models, using several iterations of biomarker subsets selection. Patients were distributed in discovery, test and validation cohorts, based on the timing of enrollment and sample collection. The discovery cohort was used for biomarker discovery and model training, the test cohort for independent model testing and selection and the validation cohort for final blinded validation of the model. To classify patients into predicted CB and predicted N-CB, we employed the SPLS (Sparse Partial Least Squares) method, which is particularly effective for small sample sizes and enhances model interpretability. The modeling process incorporated a resampling method, repeated cross-validation with 10 iterations and a repeated k-fold cross-validation of 3 for the discovery dataset. Feature reduction was performed during each modeling iteration based on the initial

feature list (DEGs) to identify the optimal model. This reduction was systematically applied by specifying feature selection within the ranges of 10, 15, and 20 features.

Each model's performance was assessed by plotting the True Positive Rate (TPR) against the False Positive Rate (FPR) at sensitivity and specificity thresholds of 90%. To classify samples as CB or N-CB, a 55% probability cut-off was used. The efficiency of the model was further verified by plotting Kaplan-Meier survival curves based on the model's predictions, along with the corresponding hazard ratios and the distance between predictive curves of responders and non-responders at 50% of the PFS. This process allowed to identify the best performing model (highest AUC and largest PFS separation) which comprised the 10 gene set. The identification of the 10 genes was therefore based on model performance upon feature selection from the DEGs identified in the longitudinal CB DEA.

Multimodal modeling

The multimodal model was optimized on the test cohort and blindly validated on the validation cohort. We did not use the discovery cohort (where the RNA model was trained) to avoid multimodal model overfitting. Specifically, for the development of a multimodal model based on RNA and ctDNA, RNA model prediction probabilities and ctDNA ratio values (ctDNA copies/mL at OT / ctDNA copies/mL at BL) were incorporated in the test cohort for thresholds optimization. Specifically, ctDNA-based predictions were adjusted using the RNA model prediction if a patient's ctDNA ratio value fell within an uncertainty range around the ctDNA ratio cutoff=1. In such case, the readout of the multimodal model for that specific patient sample would have been based on the RNA model. Vice versa, if the RNA model prediction probability was within an uncertainty range around the cut off = 55%, the multimodal model readout would have been based on the ctDNA model. If both ctDNA ratio and prediction probability were falling into the respective uncertainty ranges, the RNA model would have been prioritized in the multimodal readout. Accordingly, multiple multimodal models were created by enlarging the uncertainty ranges for both ctDNA ratio and RNA model prediction probability. Each multimodal model performance was then assessed by calculating specificity and sensitivity,

which was then compared to the standalone RNA model performance. The best combination of ctDNA ratio and predictive probability cutoffs defining the uncertainty ranges was selected in the test cohort, allowing for the highest increase in sensitivity and specificity compared to the standalone RNA model performance. Cutoffs were then applied to the validation cohort.

Statistics

Nonparametric data were analyzed by a Wilcoxon test (paired or unpaired depending on the experimental setup). $P < 0.05$ was considered as statistically significant. Differences in PFS in Kaplan-Meier curves were assessed by Mantel-Haenszel test. Each specific statistical test is reported for each experiment in the figure legends. Boxplots are used to present the data, showing median and the 25th to 75th percentiles.

Study approval

The study was conducted in accordance with relevant guidelines and regulations, and approved by the CMO Radboudumc local medical ethics committee (local registration numbers 2016-3060 and 2020-6778). Written consent was obtained from all patients for the use of biomaterials. A flow diagram of the study is presented in Figure S1A.

Data availability

Data displayed in the figures are available in the “Supporting Data Values File”. The processed ctDNA data are provided in the supplementary material. High-throughput RNA sequencing data set is deposited under the following DOI: 10.5281/zenodo.14283210 (https://zenodo.org/records/14283210). The accessibility to the next generation sequencing data generated from patient samples that support the findings of this study is restricted to protect human subject privacy and rights and preserve the scope of subjects’ consent. Data access need to be requested to the corresponding authors. All requests for raw and analyzed data will be promptly reviewed to verify if the request is subject to any intellectual property,

confidentiality obligations or privacy's restrictions to patient sensitive data. Any data and materials that can be shared will be released via a Data Transfer Agreement.

Author contributions

SVW: Conceptualization, Data curation, Formal Analysis, Funding acquisition, Validation, Investigation, Methodology, Project administration, Writing original draft - DC: Conceptualization, Data curation, Software, Formal Analysis, Supervision, Validation, Investigation, Visualisation, Methodology, Project administration, Writing original draft - SSFC: Data curation, Software, Formal Analysis, Validation, Investigation, Visualisation, Methodology - IBAWTP: Data curation, Formal Analysis, Validation, Investigation, Methodology - SHT: Data curation, Formal Analysis, Investigation, Methodology - JVI: Resources, Investigation, Methodology - LIK: Resources, Investigation, Methodology - SP: Resources, Data curation - SMB: Resources, Data curation - GC: Resources, Data curation - NH: Software, Methodology- IMO: Resources - TJS: Resources - TVV: Resources - MB: Resources - MDF: Resources - MJLL: Supervision - SHE: Conceptualization, Supervision, Funding acquisition, Investigation, Project administration - LC: Conceptualization, Data curation, Supervision, Funding acquisition, Validation, Investigation, Methodology, Project administration - PR: Conceptualization, Supervision - NM: Conceptualization, Resources, Funding acquisition, Validation, Investigation, Methodology, Project administration

SVW, DC, SSFC equal contribution order was defined by random choice.

652 **Acknowledgments**

653 This research was supported by a Eurostars grant (E! 114908 - PRECISE) and Paul Speth

654 Foundation (Bullseye project). Our particular gratitude is extended to all patients who generously donated samples for analyses, and without whom this study would not have been possible.

References

1. Bellmunt J, de Wit R, Vaughn DJ, Fradet Y, Lee JL, Fong L, et al. Pembrolizumab as Second-Line Therapy for Advanced Urothelial Carcinoma. New England Journal of Medicine. 2017 Mar;376(11):1015–26.
2. Powles T, Park SH, Voog E, Caserta C, Valderrama BP, Gurney H, et al. Avelumab Maintenance Therapy for Advanced or Metastatic Urothelial Carcinoma. https://doi.org/101056/NEJMoa2002788 [Internet]. 2020 Sep 18 [cited 2021 Aug 11];383(13):1218–30. Available from: https://www.nejm.org/doi/full/10.1056/NEJMoa2002788
3. Powles T, Bellmunt J, Comperat E, De Santis M, Huddart R, Loriot Y, et al. ESMO Clinical Practice Guideline interim update on first-line therapy in advanced urothelial carcinoma. Annals of Oncology. 2024 Jun;35(6):485–90.
4. Powles T, Valderrama BP, Gupta S, Bedke J, Kikuchi E, Hoffman-Censits J, et al. Enfortumab Vedotin and Pembrolizumab in Untreated Advanced Urothelial Cancer. New England Journal of Medicine. 2024 Mar 7;390(10):875–88.
5. van der Heijden MS, Sonpavde G, Powles T, Necchi A, Burotto M, Schenker M, et al. Nivolumab plus Gemcitabine–Cisplatin in Advanced Urothelial Carcinoma. New England Journal of Medicine. 2023 Nov 9;389(19):1778–89.
6. Balar A V, Castellano D, O'Donnell PH, Grivas P, Vuky J, Powles T, et al. First-line pembrolizumab in cisplatin-ineligible patients with locally advanced and unresectable or metastatic urothelial cancer (KEYNOTE-052): a multicentre, single-arm, phase 2 study. Lancet Oncol [Internet]. 2017 Nov [cited 2019 Oct 2];18(11):1483–92. Available from: https://linkinghub.elsevier.com/retrieve/pii/S1470204517306162
7. Balar AV, Castellano DE, Grivas P, Vaughn DJ, Powles T, Vuky J, et al. Efficacy and safety of pembrolizumab in metastatic urothelial carcinoma: results from KEYNOTE-045 and KEYNOTE-052 after up to 5 years of follow-up. Annals of Oncology. 2023 Mar;34(3):289–99.
8. Powles T, Durán I, van der Heijden MS, Loriot Y, Vogelzang NJ, De Giorgi U, et al. Atezolizumab versus chemotherapy in patients with platinum-treated locally advanced or metastatic urothelial carcinoma (IMvigor211): a multicentre, open-label, phase 3 randomised controlled trial. The Lancet [Internet]. 2018 Feb 24 [cited 2021 Feb 11];391(10122):748–57. Available from: https://pubmed.ncbi.nlm.nih.gov/29268948/
9. Powles T, Kockx M, Rodriguez-Vida A, Duran I, Crabb SJ, Van Der Heijden MS, et al. Clinical efficacy and biomarker analysis of neoadjuvant atezolizumab in operable urothelial carcinoma in the ABACUS trial. Nat Med [Internet]. 2019 Nov 1 [cited 2021 Jun 25];25(11):1706–14. Available from: https://pubmed.ncbi.nlm.nih.gov/31686036/
10. Necchi A, Anichini A, Raggi D, Briganti A, Massa S, Lucianò R, et al. Pembrolizumab as Neoadjuvant Therapy Before Radical Cystectomy in Patients With Muscle-Invasive Urothelial Bladder Carcinoma (PURE-01): An Open-Label, Single-Arm, Phase II Study. J Clin Oncol [Internet]. 2018 Oct 20 [cited 2019 Oct 2];36(34):JCO1801148. Available from: http://ascopubs.org/doi/10.1200/JCO.18.01148

11. Samstein RM, Lee CH, Shoushtari AN, Hellmann MD, Shen R, Janjigian YY, et al. Tumor mutational load predicts survival after immunotherapy across multiple cancer types. Nat Genet [Internet]. 2019 Feb 1 [cited 2021 Dec 19];51(2):202–6. Available from: https://pubmed.ncbi.nlm.nih.gov/30643254/

12. Rui X, Gu TT, Pan HF, Zhang HZ. Evaluation of PD-L1 biomarker for immune checkpoint inhibitor (PD-1/PD-L1 inhibitors) treatments for urothelial carcinoma patients: A meta-analysis. Int Immunopharmacol. 2019 Feb;67:378–85.

13. Kilgour E, Rothwell DG, Brady G, Dive C. Liquid Biopsy-Based Biomarkers of Treatment Response and Resistance. Cancer Cell. 2020 Apr 13;37(4):485–95.

14. Powles T, Chang YH, Yamamoto Y, Munoz J, Reyes-Cosmelli F, Peer A, et al. Pembrolizumab for advanced urothelial carcinoma: exploratory ctDNA biomarker analyses of the KEYNOTE-361 phase 3 trial. Nat Med. 2024 Jun 1;

15. Tolmeijer SH, van Wilpe S, Geerlings MJ, von Rhein D, Smilde TJ, Kloots ISH, et al. Early On-treatment Circulating Tumor DNA Measurements and Response to Immune Checkpoint Inhibitors in Advanced Urothelial Cancer. Eur Urol Oncol [Internet]. 2023 Sep [cited 2023 Oct 1]; Available from: https://pubmed.ncbi.nlm.nih.gov/37673768/

16. Herbst RS, Soria JC, Kowanetz M, Fine GD, Hamid O, Gordon MS, et al. Predictive correlates of response to the anti-PD-L1 antibody MPDL3280A in cancer patients. Nature. 2014 Nov 27;515(7528):563–7.

17. Strickler JH, Hanks BA, Khasraw M. Tumor Mutational Burden as a Predictor of Immunotherapy Response: Is More Always Better? Clinical Cancer Research. 2021 Mar 1;27(5):1236–41.

18. Fairfax BP, Taylor CA, Watson RA, Nassiri I, Danielli S, Fang H, et al. Peripheral CD8+ T cell characteristics associated with durable responses to immune checkpoint blockade in patients with metastatic melanoma. Nat Med [Internet]. 2020 Feb 1 [cited 2021 Dec 18];26(2):193. Available from: /pmc/articles/PMC7611047/

19. Luoma AM, Suo S, Wang Y, Gunasti L, Porter CBM, Nabilsi N, et al. Tissue-resident memory and circulating T cells are early responders to pre-surgical cancer immunotherapy. Cell. 2022 Aug;185(16):2918-2935.e29.

20. van Wilpe S, Wosika V, Ciarloni L, Ehrensberger SH, Jeitziner R, Angelino P, et al. Whole Blood Transcriptome Profiling Identifies DNA Replication and Cell Cycle Regulation as Early Marker of Response to Anti-PD-1 in Patients with Urothelial Cancer. Cancers (Basel) [Internet]. 2021 Sep 1 [cited 2021 Dec 16];13(18). Available from: https://pubmed.ncbi.nlm.nih.gov/34572887/

21. Hendrickx W, Simeone I, Anjum S, Mokrab Y, Bertucci F, Finetti P, et al. Identification of genetic determinants of breast cancer immune phenotypes by integrative genome-scale analysis. Oncoimmunology [Internet]. 2017 Feb 1 [cited 2024 Feb 29];6(2). Available from: https://pubmed.ncbi.nlm.nih.gov/28344865/

22. Seitz RS, Hurwitz ME, Nielsen TJ, Bailey DB, Varga MG, Ring BZ, et al. Translation of the 27-gene immuno-oncology test (IO score) to predict outcomes in immune checkpoint inhibitor treated metastatic urothelial cancer patients. J

Transl Med [Internet]. 2022 Dec 1 [cited 2023 Sep 25];20(1). Available from: https://pubmed.ncbi.nlm.nih.gov/35974414/

23. Reijers ILM, Rao D, Versluis JM, Menzies AM, Dimitriadis P, Wouters MW, et al. IFN-γ signature enables selection of neoadjuvant treatment in patients with stage III melanoma. Journal of Experimental Medicine [Internet]. 2023 May 1 [cited 2023 Oct 2];220(5). Available from: https://doi.org/10.1084/jem.20221952

24. Argelaguet R, Velten B, Arnol D, Dietrich S, Zenz T, Marioni JC, et al. Multi-Omics Factor Analysis—a framework for unsupervised integration of multi-omics data sets. Mol Syst Biol. 2018 Jun 20;14(6).

25. Sammut SJ, Crispin-Ortuzar M, Chin SF, Provenzano E, Bardwell HA, Ma W, et al. Multi-omic machine learning predictor of breast cancer therapy response. Nature. 2022 Jan 27;601(7894):623–9.

26. Seymour L, Bogaerts J, Perrone A, Ford R, Schwartz LH, Mandrekar S, et al. iRECIST: guidelines for response criteria for use in trials testing immunotherapeutics [Internet]. Vol. 18, The Lancet Oncology. Lancet Publishing Group; 2017 [cited 2021 Apr 12]. p. e143–52. Available from: /pmc/articles/PMC5648544/

27. Raja R, Kuziora. M, Brohawn P, Higgs B, Gupta A, Dennis P, et al. Early Reduction in ctDNA Predicts Survival in Patients with Lung and Bladder Cancer Treated with Durvalumab. Clin Cancer Res [Internet]. 2018 Dec 15 [cited 2021 Sep 24];24(24):6212–22. Available from: https://pubmed.ncbi.nlm.nih.gov/30093454/

28. Powles T, Chang YH, Yamamoto Y, Munoz J, Reyes-Cosmelli F, Peer A, et al. Pembrolizumab for advanced urothelial carcinoma: exploratory ctDNA biomarker analyses of the KEYNOTE-361 phase 3 trial. Nat Med. 2024 Jun 1;

29. Goldberg SB, Narayan A, Kole AJ, Decker RH, Teysir J, Carriero NJ, et al. Early Assessment of Lung Cancer Immunotherapy Response via Circulating Tumor DNA. Clin Cancer Res. 2018 Apr 15;24(8):1872–80.

30. Herbreteau G, Langlais A, Greillier L, Audigier-Valette C, Uwer L, Hureaux J, et al. Circulating Tumor DNA as a Prognostic Determinant in Small Cell Lung Cancer Patients Receiving Atezolizumab. J Clin Med. 2020 Nov 27;9(12):3861.

31. Váraljai R, Wistuba-Hamprecht K, Seremet T, Diaz JMS, Nsengimana J, Sucker A, et al. Application of Circulating Cell-Free Tumor DNA Profiles for Therapeutic Monitoring and Outcome Prediction in Genetically Heterogeneous Metastatic Melanoma. JCO Precis Oncol. 2020;3.

32. Anagnostou V, Forde PM, White JR, Niknafs N, Hruban C, Naidoo J, et al. Dynamics of Tumor and Immune Responses during Immune Checkpoint Blockade in Non–Small Cell Lung Cancer. Cancer Res. 2019 Mar 15;79(6):1214–25.

33. Kansara M, Bhardwaj N, Thavaneswaran S, Xu C, Lee JK, Chang LB, et al. Early circulating tumor DNA dynamics as a pan-tumor biomarker for long-term clinical outcome in patients treated with durvalumab and tremelimumab. Mol Oncol. 2023 Feb;17(2):298–311.

34. Raja R, Kuziora M, Brohawn PZ, Higgs BW, Gupta A, Dennis PA, et al. Early Reduction in ctDNA Predicts Survival in Patients with Lung and Bladder Cancer

Treated with Durvalumab. Clinical Cancer Research. 2018 Dec 15;24(24):6212–22.

35. Richard C, Chevrier S, Marabelle A, Boidot R. Abstract 7611: Circulating blood RNAseq detects activation of immune system and predicts response to immunotherapy in bladder cancer. Cancer Res. 2024 Mar 22;84(6_Supplement):7611–7611.

36. Huang AC, Postow MA, Orlowski RJ, Mick R, Bengsch B, Manne S, et al. T-cell invigoration to tumour burden ratio associated with anti-PD-1 response. Nature [Internet]. 2017 May 10 [cited 2019 Aug 2];545(7652):60–5. Available from: http://www.nature.com/articles/nature22079

37. Galsky MD, Sonpavde GP, Powles T, Claps M, Burotto M, Schenker M, et al. Characterization of complete responders to nivolumab + gemcitabine-cisplatin vs gemcitabine-cisplatin alone and patients with lymph node–only metastatic urothelial carcinoma from the CheckMate 901 trial. Journal of Clinical Oncology. 2024 Jun 1;42(16_suppl):4509–4509.

38. Schwartz LH, Litière S, de Vries E, Ford R, Gwyther S, Mandrekar S, et al. RECIST 1.1—Update and clarification: From the RECIST committee. Eur J Cancer [Internet]. 2016 Jul 1 [cited 2020 Apr 19];62:132–7. Available from: https://linkinghub.elsevier.com/retrieve/pii/S0959804916320433

39. Agarwal N, Bellmunt J, Maughan BL, Boucher KM, Choueiri TK, Qu AQ, et al. Six-month progression-free survival as the primary endpoint to evaluate the activity of new agents as second-line therapy for advanced urothelial carcinoma. Clin Genitourin Cancer [Internet]. 2014 [cited 2024 Nov 28];12(2):130–7. Available from: https://pubmed.ncbi.nlm.nih.gov/24220220/

40. Annala M, Vandekerkhove G, Khalaf D, Taavitsainen S, Beja K, Warner EW, et al. Circulating Tumor DNA Genomics Correlate with Resistance to Abiraterone and Enzalutamide in Prostate Cancer. Cancer Discov. 2018 Apr 1;8(4):444–57.

Figures

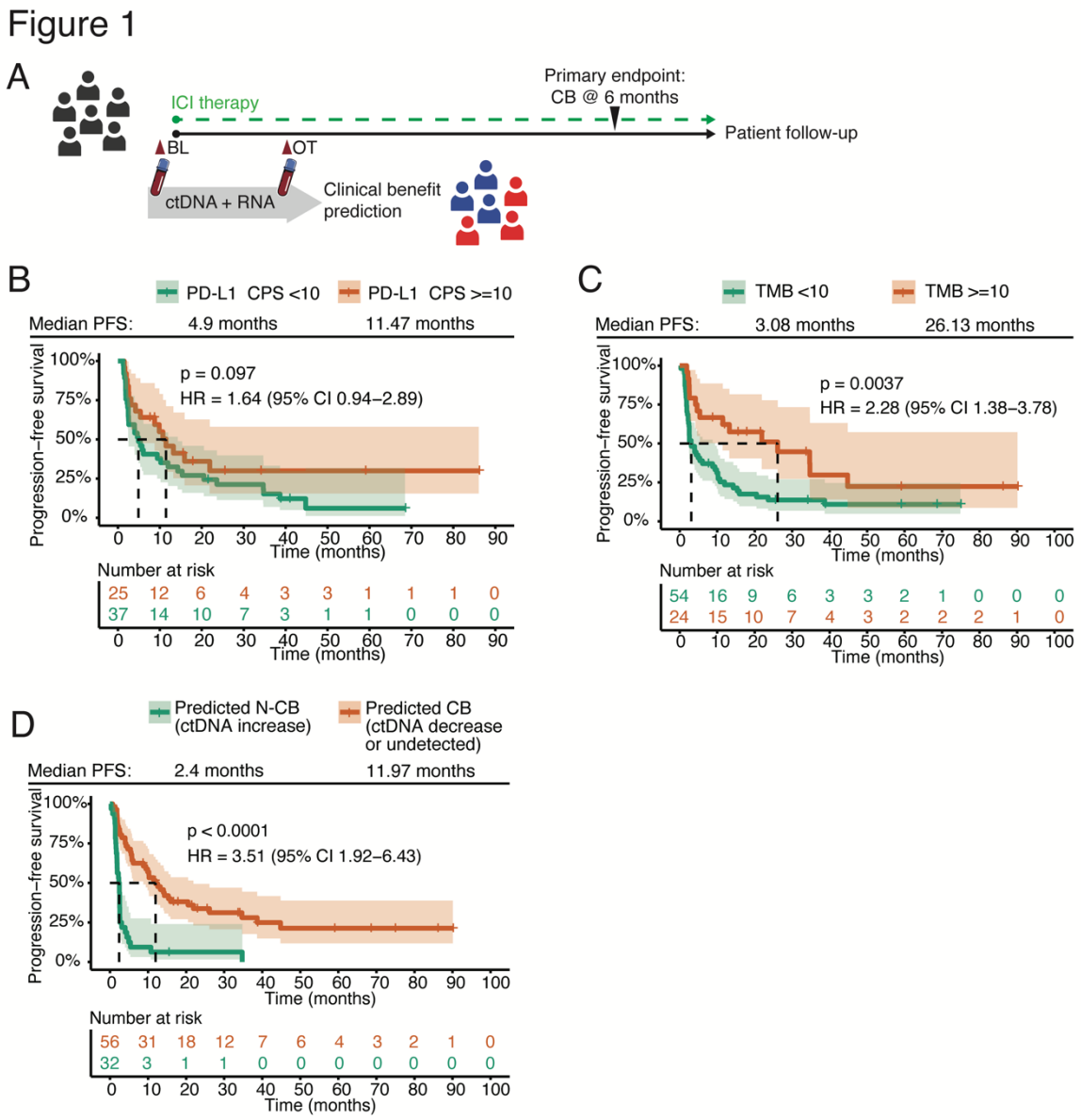

Figure 1 – circulating tumor DNA (ctDNA) dynamics predicts clinical benefit (CB) to immune-checkpoint inhibitor (ICI) therapy in metastatic urothelial cancer (mUC) patients: A) Sample collection and analysis schematic: mUC patients were treated with ICI (either pembrolizumab, nivolumab or avelumab) until disease progression. Blood was collected at baseline (BL, before cycle 1) and on-treatment (OT, after 2-6 weeks) for both ctDNA and RNA analysis. The primary endpoint was CB. This was defined as progression-free survival for at least 6 months. **B)** Kaplan-Meier (KM) curve comparing the progression-free survival (PFS) of patients with PD-L1 positive tumor (orange curve, PD-L1 combined positive score

828 ≥10) and patients with PD-L1 negative tumor (green curve, PD-L1 combined positive score
829 <10). **C)** KM curve comparing the PFS of patients with a high tumor mutational burden (TMB)
830 (orange curve, TMB ≥10 mutations/Mb) and TMB low patients (green curve, TMB <10). **D)** KM
831 curve comparing the PFS of ctDNA-based patient stratification. The predicted CB population
832 (orange curve) contains patients who had a decrease of ctDNA fraction from BL to OT or
833 undetected at both timepoints. The predicted non-clinical benefit (N-CB, green curve)
834 population contains patients where the ctDNA fraction increased from BL to OT or was stable.
835 **Statistics:** p = p-value as determined by a Mantel-Haenszel test, HR = hazard ratio, CI =
836 confidence interval.

Figure S1

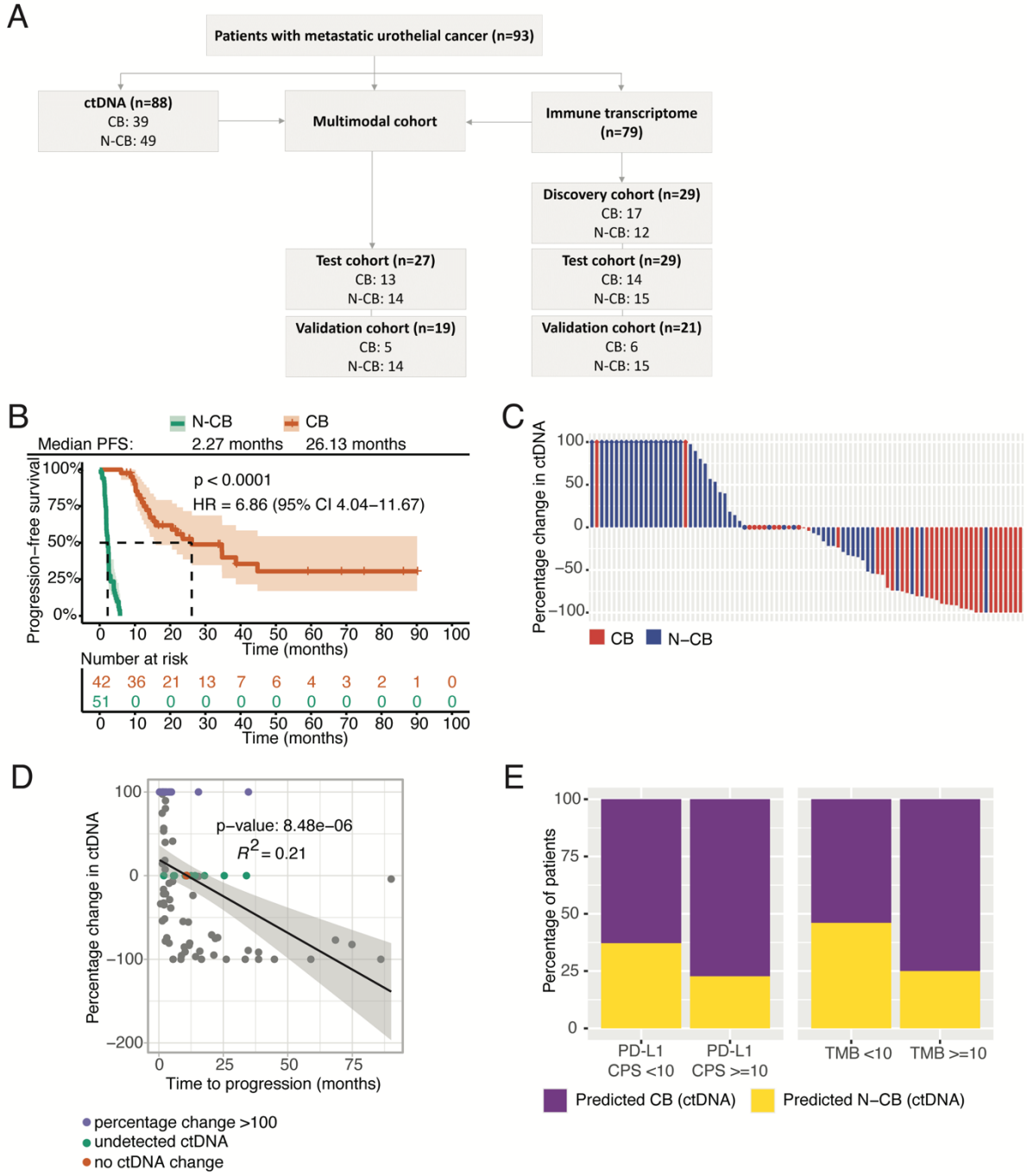

Figure S1 – clinical characteristics of ICI-treated mUC patients: A) Diagram describing the different cohorts used in the study. For each cohort, the number of patients with (CB) and without clinical benefit (N-CB) is annotated. **B)** KM curve comparing the PFS of the CB and N-CB groups. **C)** Baseline to on-treatment percentage change in ctDNA levels. Each bar represents a patient, asterisks represent patients with undetected ctDNA at both timepoints and dots represent patients with no ctDNA change. Arrows indicate a percentage change

844 >100. CB group is annotated (red=CB, blue=N-CB). **D)** Correlation between the percentage
845 change of ctDNA fraction and time to progression. Violet dots highlight patients with a
846 percentage change >100, green dots patients with undetected ctDNA at both timepoints, and
847 orange dots patients with no ctDNA change. Linear regression analysis was performed to
848 examine the relationship. The regression line (black), confidence intervals (gray), R^2 value and
849 p-value are displayed on the plot. **E)** Distribution of ctDNA-based patient predictions into PD-
850 L1 CPS (left) and TMB categories (right). **Statistics:** p = p-value as determined by a Mantel-
851 Haenszel test, HR = hazard ratio, CI = confidence interval.
852

Figure 2

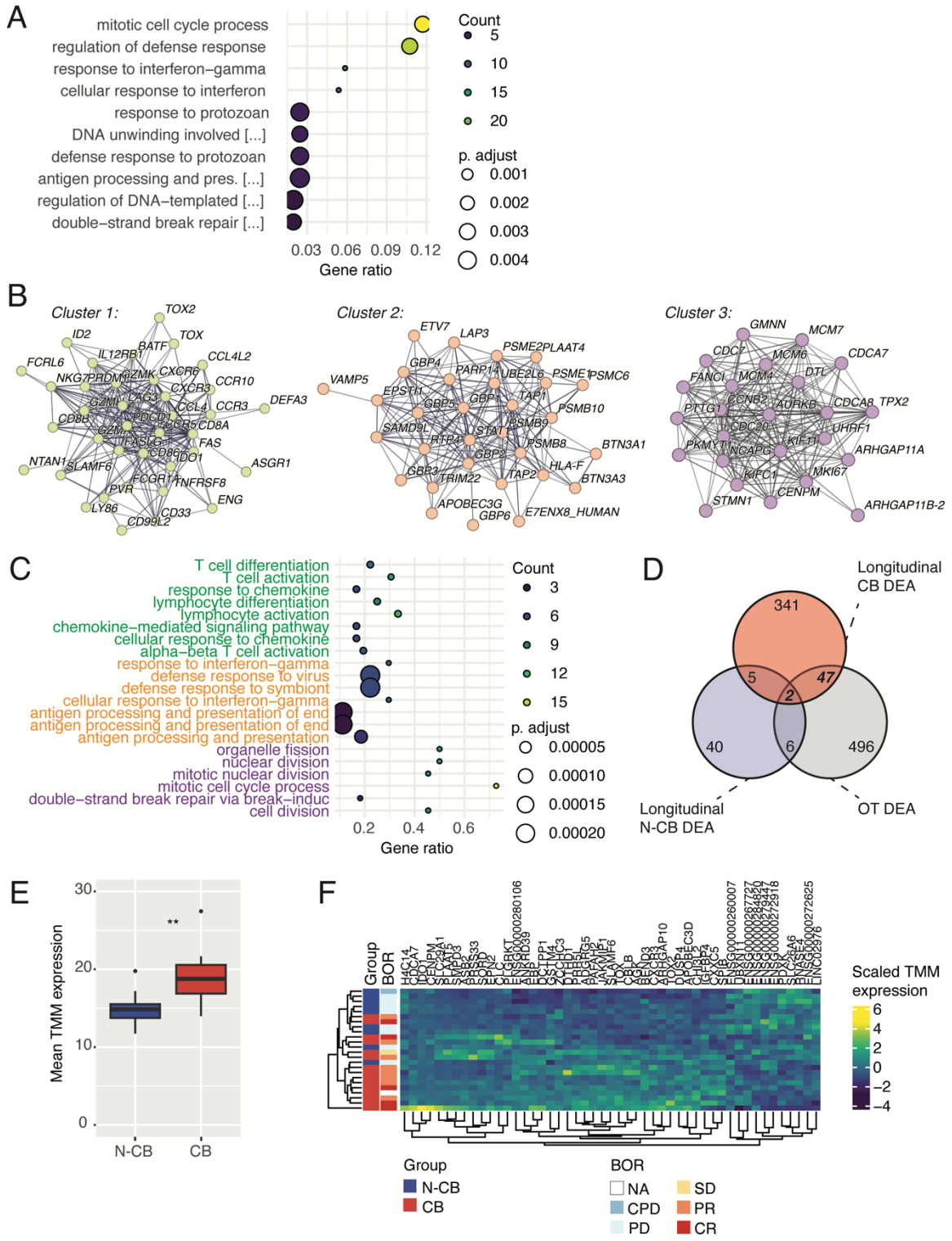

Figure 2 – blood immunotranscriptome dynamics in CB patients reveal the biological mode-of-action of early response to ICI: A) Over-representation analysis (ORA) performed on the up-regulated differentially expressed genes at OT (edgeR fold-change >0) found by

differential expression analysis (DEA) comparing paired BL to OT samples of CB patients (longitudinal CB DEA). The top enriched gene ontology biological processes (GO BPs) are shown (based on an enrichment adjusted p-value ≤0.05), highlighting pathways up-regulated at OT. **B)** Largest gene clusters identified by STRING analysis of all DEGs in the longitudinal CB DEA. Each node represents a gene and each segment an interaction defined by STRING analysis. **C)** ORA performed on the genes included in the clusters showed in B). The top GO BPs are shown (based on an enrichment adjusted p-value ≤0.05, green terms are associated to cluster 1, orange terms to cluster 2 and violet terms to cluster 3). **D)** Venn diagram showing the DEGs intersect between the longitudinal CB DEA (395 DEGs), the DEA comparing paired BL to OT samples of N-CB patients (longitudinal N-CB DEA, 53 DEGs) and the DEA comparing CB to N-CB patients at OT timepoint (OT DEA, 551 DEGs). The 49-gene intersect between the longitudinal CB DEA to the OT DEA is highlighted. **E)** Boxplot comparing the mean expression of the 49-gene set highlighted in D) in the N-CB and CB patient group at OT timepoint. Gene expression is defined for each patient by the mean of the trimmed mean of M values (TMM) for each gene in the 49-gene set. **F)** Expression heat map and hierarchical clustering of the 49-gene set in N-CB and CB patients at OT timepoint. Columns and rows are hierarchically clustered. Patient group and best overall response (BOR) are annotated per row. NA = not annotated, CPD = clinical progressive disease, PD = progressive disease, SD = stable disease, PR = partial response, CR = complete response. **Statistics:** ** p-value <0.01 by Wilcoxon test.

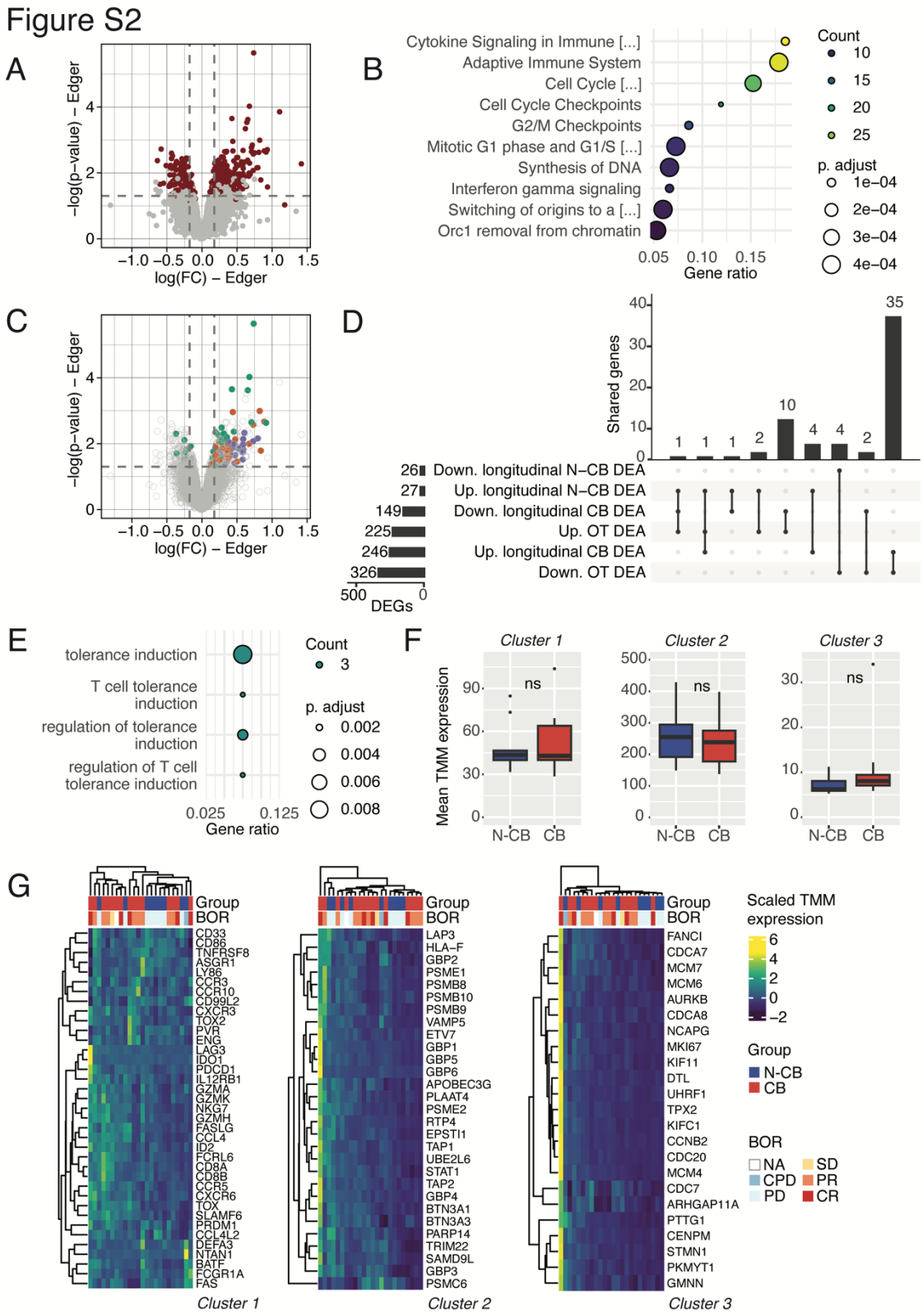

877

878 **Figure S2 – ICI therapy induces T-cell signaling and cell proliferation in blood: A)**

879 Volcano plot analysis of the RNA sequencing (RNA-seq) data depicting log2 fold change (FC,

880 based on edgeR, x-axis) versus significance (-log10(p-value), based on edgeR, y-axis) for the

longitudinal CB DEA. Each dot represents a gene and DEGs are highlighted in red. **B)** ORA performed on the up-regulated differentially expressed genes (DEGs) at OT found by the longitudinal CB DEA. The top enriched pathways are shown (based on an enrichment adjusted p-value ≤0.05), in this case using the Reactome ontology, highlighting up-regulated pathways at OT. **C)** Volcano plot analysis as in figure S2A, where genes belonging to the identified STRING network clusters are highlighted (green=cluster 1, orange=cluster 2 and violet=cluster 3). **D)** UpSet plot comparing up- and down-regulated DEGs (based on edgeR FC≥0 or <0, respectively) of the longitudinal CB DEA, the longitudinal N-CB DEA and the OT DEA (comparing the CB and N-CB group at OT). **E)** ORA performed on the 49-gene intersect between the longitudinal CB DEA to the OT DEA. The top enriched GO BPs are shown (based on an enrichment adjusted p-value ≤0.05). **F)** Boxplot comparing the mean expression of the gene STRING clusters 1, 2 and 3 (described in Figure 2B and C) in the N-CB and CB patient group at OT timepoint. Gene expression is defined for each patient by the mean of the trimmed mean of M values (TMM) for each gene cluster. **G)** Expression heat map and hierarchical clustering of the gene STRING clusters 1, 2 and 3 (described in Figure 2B and C) in the N-CB and CB patient group at OT timepoint. Columns and rows are hierarchically clustered. Patient group and best overall response (BOR) are annotated per column. NA = not annotated, CPD = clinical progressive disease, PD = progressive disease, SD = stable disease, PR = partial response, CR = complete response. **Statistics:** ns = not significant by Wilcoxon test.

Figure 3

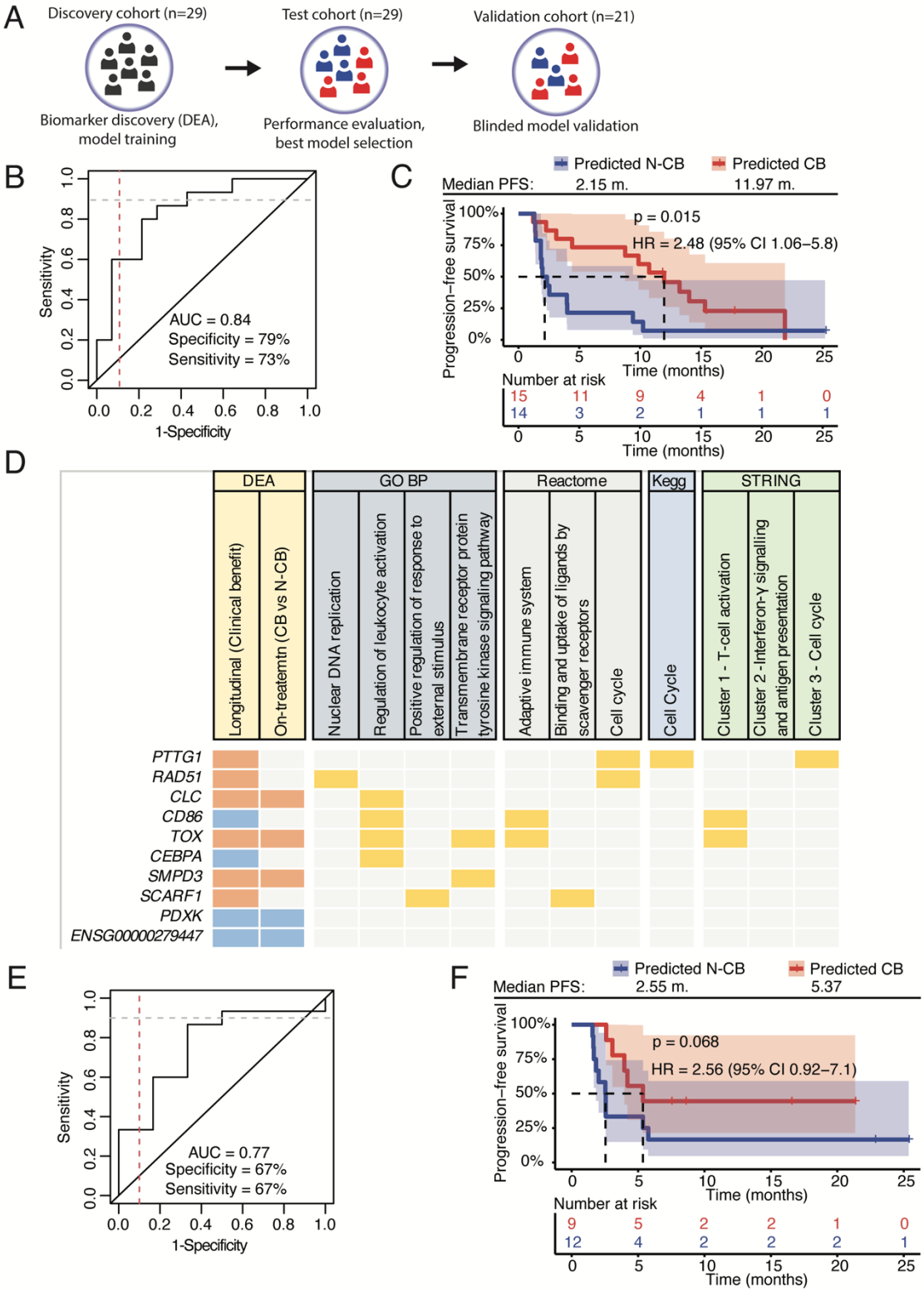

Figure 3 – Blood-based immunotranscriptome predictive model forecasts CB in an independent cohort: A) Modelling approach schematic: biomarker discovery was performed in the discovery cohort (patients with paired BL and OT RNA-seq data, N=29) by DEA. Model

training was performed in the same cohort by multiple iterations of random features reduction of the biomarker/gene list, followed by model testing in the independent test cohort (patients with paired BL and OT RNA-seq data, N=29). The best CB predictive model was selected by area under the curve (AUC) ranking of each model receiver operating characteristics curve (ROC) and by ranking the difference in median PFS between the predicted CB and N-CB groups in the test cohort (N=29). Last, the best performing model was validated in the validation cohort (patients with paired BL and OT RNA-seq data, N=21). **B)** Receiver-operating characteristics (ROC) curve showing model performance of the best performing model in the independent test cohort (N=29). Specificity is calculated with respect to CB patients (true negative cases), while sensitivity to N-CB (true positive cases). **C)** KM curve comparing the PFS of model-based predicted CB population (red) and predicted N-CB population (blue) in the independent test cohort (N=29). **D)** Attention map contextualizing the biology of the 10 genes used to craft the model shown in B) and C) showing in which DEA the genes were identified. The genes have also been mapped to a selection of significantly enriched pathways of different ontologies in the longitudinal CB DEA (enrichment adjusted p-value ≤0.05) and to the STRING network clusters shown in Figure 2B. Genes included in the DEGs of the longitudinal CB DEA or the OT DEA are highlighted in orange (up-regulated, based on edgeR FC≥0) or in blue (down-regulated, based on edgeR FC<0). Genes associated to enriched pathways or STRING clusters are highlighted in yellow. **E)** ROC curve showing model performance assessment in the independent blinded validation cohort (N=21). Specificity is calculated with respect to CB patients (true negative cases) and sensitivity to N-CB (true positive cases). **F)** KM curve comparing the PFS of RNA model-based predicted CB population (red) and N-CB population (blue) in the independent blinded validation cohort (N=21). **Statistics:** p = p-value as determined by a Mantel-Haenszel test, HR = hazard ratio (predicted CB population as reference), CI = confidence interval.

Figure S3

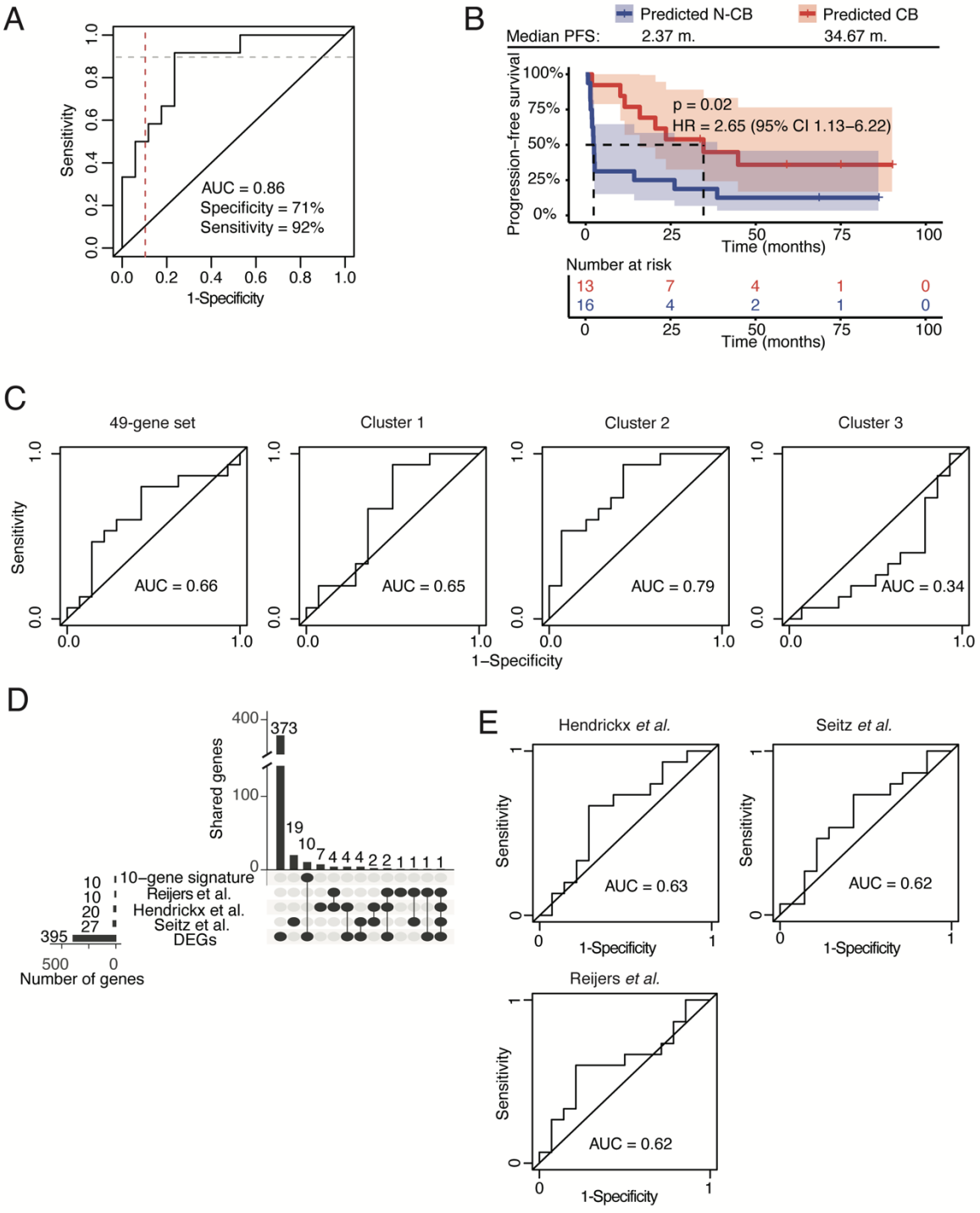

930

931 **Figure S3 – The unique 10-gene panel model outperforms other gene signatures: A)**
932 ROC curve showing model performance in the discovery cohort (N=29). Specificity is
933 calculated with respect to CB patients (true negative cases), while sensitivity to N-CB (true
934 positive cases). **B)** KM curve comparing the PFS of model-based predicted CB population (red)
935 and predicted N-CB population (blue) in the discovery cohort (N=29). **C)** ROCs showing the

performance in the independent test cohort of CB predictive models crafted with the 49-gene intersect and STRING network gene lists. **D)** Upset plot comparing the DEGs of the longitudinal CB DEA and the 10-gene panel to relevant literature-based tumor-derived gene signatures that have been described to be associated with CB to ICI in other studies (21–23). **E)** ROCs showing the performance in the independent test cohort of CB predictive models crafted with literature-based gene lists. **Statistics:** p = p-value as determined by a Mantel-Haenszel test, HR = hazard ratio (predicted CB population as reference), CI = confidence interval.

Figure 4

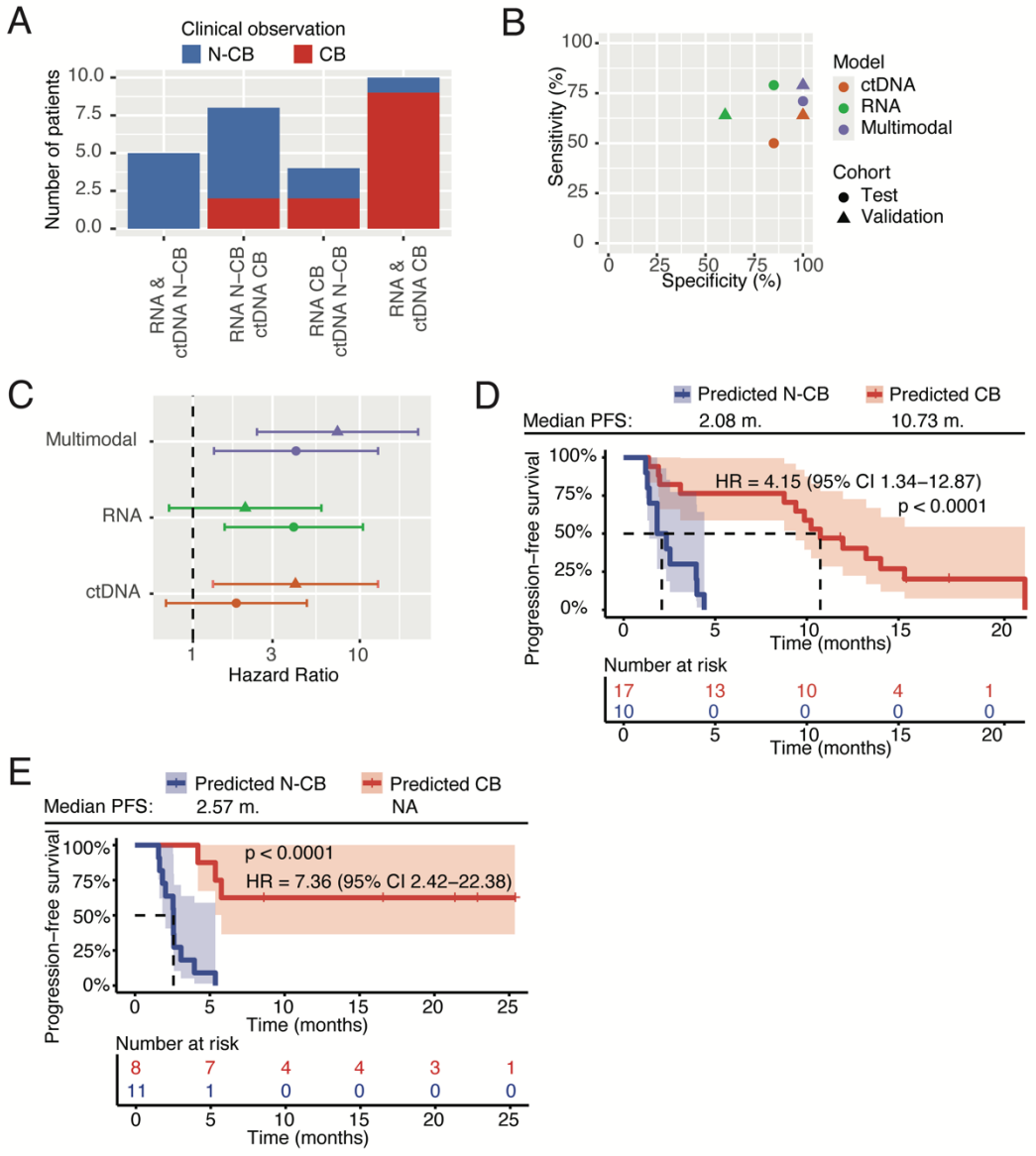

Figure 4 – integration of ctDNA- and RNA-based biomarkers boosts the performance of a multimodal model in an independent blinded validation cohort: A) Prediction comparison: patients of the independent test cohort (N=27, where both RNAseq and ctDNA data were available) were categorized based on the RNA and ctDNA model predictions, highlighting convergent or divergent readouts by the two approaches. Columns' color-coding reflects the actual CB group defined by clinical assessment (red=CB, blue=N-CB). **B)** Model performance comparison of the different model approaches (ctDNA model in orange, RNA model in green, multimodal model in violet) in the independent test cohort (circles, N=27, where both RNAseq and ctDNA data were available) and blinded validation cohort (triangles, N=19,

where both RNAseq and ctDNA data were available). **C)** Hazard Ratio (HR) for PFS of the three modelling approaches used for patient stratification (ctDNA model in orange, RNA model in green, multimodal model in violet) in the independent test (circles, N=27, where both RNAseq and ctDNA data were available) and blinded validation cohorts (triangles, N=19, where both RNAseq and ctDNA data were available). The bars represent the confidence of interval for each HR. The dashed line represents a HR=1. **D)** KM curve comparing the PFS of the multimodal model-based predicted CB population (red) and N-CB population (blue) in the independent test cohort (N=27, where both RNAseq and ctDNA data were available) and **E)** in an additional blinded and independent validation cohort (N=19, where both RNAseq and ctDNA data were available). **Statistics:** p = p-value as determined by a Mantel-Haenszel test, HR = hazard ratio (predicted CB population as reference), CI = confidence interval.

Figure S4

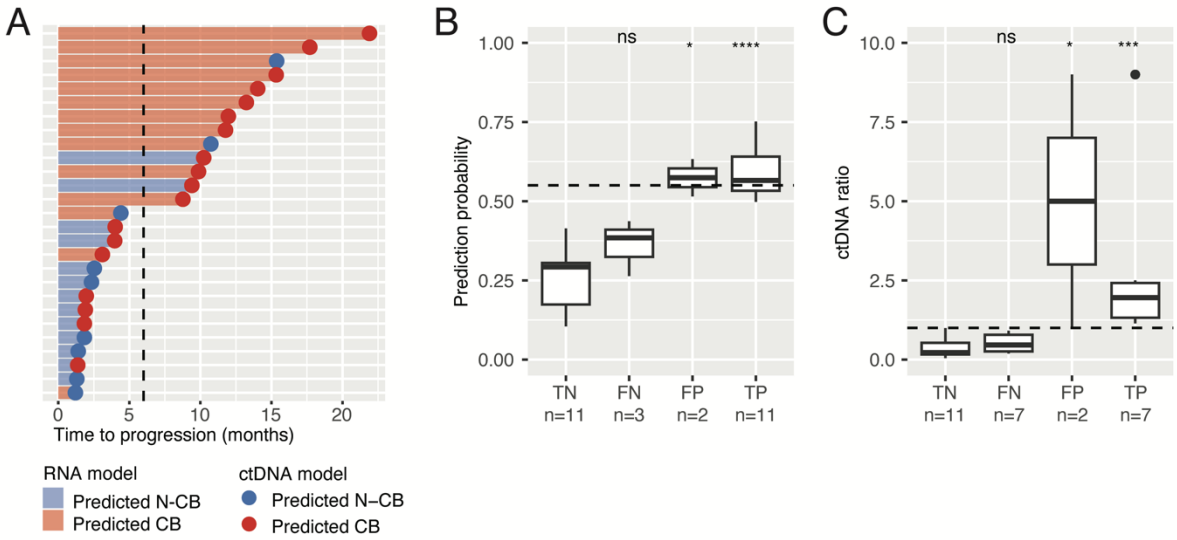

Figure S4 – optimization of RNA and ctDNA prediction cutoffs: A) Swimmer plot showing the individual time to progression of patients in the independent test cohort (N=27, where both RNAseq and ctDNA data were available). Each bar represents a patient. The dashed line indicates a PFS of 6 months, which has been used as clinical endpoint to define CB and N-CB. Red bars represent patients with predicted CB based on the immunotranscriptome predictive model (RNA model), while blue bars represent patients with predicted N-CB by the RNA model. Circles represent the ctDNA-based prediction for each patient, respectively CB (red circle) or N-CB (blue circle). **B)** Prediction probability of true negative (TN), false negative (FN), false positive (FP) and true positive (TP) predictions of the RNA model. The dashed line represents the prediction probability cutoff used for prediction calling. **C)** CtDNA ratio of true negative (TN), false negative (FN), false positive (FP) and true positive (TP) predictions of the ctDNA model. The dashed line represents the ctDNA ratio cutoff used for prediction calling. **Statistics:** ns = not significant, * p-value <0.05, *** p-value <0.001, **** p-value <0.0001 by Wilcoxon test.

Tables

Table 1. Baseline patient characteristics

	Total cohort (N=93)	ctDNA cohort (N=88)	RNAseq cohort (N=79) discovery (N=29)	test (N=29)	validation (N=21)	MMM validation (N=19)
Age at baseline (yr), median (range)	69 (34-85)	69 (34-89)	67 (39-79)	69 (34-85)	64 (35-81)	66 (25-81)
Sex, n (%)						
Female	19 (20.4)	19 (21.6)	6 (20.7)	6 (20.7)	5 (23.8)	5 (26.3)
Male	74 (79.6)	69 (78.4)	23 (79.3)	23 (79.3)	16 (76.2)	14 (73.7)
Upper tract, N (%)						
Yes	14 (15.1)	14 (15.9)	3 (10.3)	5 (17.2)	4 (19.0)	4 (21.1)
No	74 (79.6)	70 (79.5)	23 (79.3)	22 (75.9)	17 (81.0)	15 (78.9)
Unknown	5 (5.4)	4 (4.5)	3 (10.3)	2 (6.9)	0 (0)	0 (0)
Metastatic at diagnosis, N (%)	27 (29.0)	25 (28.4)	4 (13.8)	13 (44.8)	7 (33.3)	7 (36.8)
Immunotherapy, N (%)						
Pembrolizumab	72 (77.4)	67 (76.1)	22 (75.9)	23 (79.3)	16 (76.2)	14 (73.7)
Nivolumab	7 (7.5)	7 (8.0)	7 (24.1)	0 (0)	0 (0)	0 (0)
Avelumab	14 (15.1)	14 (15.9)	0 (0)	6 (20.7)	5 (23.8)	5 (26.3)
Systemic treatment before immunotherapy, N (%)						
Gemcitabin/ carboplatin	33 (35.5)	31 (35.2)	15 (51.7)	10 (34.5)	8 (38.1)	8 (42.1)
Gemcitabin/ cisplatin	37 (39.8)	35 (39.8)	9 (31.0)	12 (41.4)	6 (28.6)	5 (26.3)
MVAC, dose dense	3 (3.2)	3 (3.4)	2 (6.9)	1 (3.4)	0 (0)	0 (0)
Pembrolizumab	2 (2.2)	2 (2.3)	0 (0)	1 (3.4)	1 (4.8)	1 (5.3)

None	21 (22.6)	20 (22.7)	4 (13.8)	7 (24.1)	6 (28.6)	6 (31.6)
Other	5 (5.4)	5 (5.7)	2 (6.9)	1 (3.4)	2 (9.5)	2 (10.5)
ECOG performance status, N (%)						
0	12 (12.9)	12 (13.6)	3 (10.3)	7 (24.1)	0 (0)	1 (5.3)
1	58 (62.4)	54 (61.4)	19 (65.5)	16 (55.2)	13 (61.9)	12 (63.2)
2	16 (17.2)	16 (18.2)	7 (24.1)	5 (17.2)	2 (9.5)	2 (10.5)
Unknown	7 (7.5)	6 (6.8)	0 (0)	1 (3.4)	5 (23.8)	4 (21.1)
Presence of visceral metastasis at baseline, N (%)	42 (45.2)	38 (43.2)	13 (44.8)	9 (31.0)	13 (61.9)	11 (57.9)
Presence of liver metastasis at baseline, N (%)	19 (20.4)	17 (19.3)	7 (24.1)	5 (17.2)	5 (23.8)	4 (21.1)
Timing on-treatment blood sample, N (%)[A]						
2-4 weeks		74 (84.1)	23 (79.3)	20 (69.0)	17 (81.0)	16 (84.2)
6 weeks[B]		14 (15.9)	6 (20.7)	9 (31.0)	4 (19.0)	3 (15.8)
Tumor mutational burden (nonsynonymous mutations/Mb), N (%)						
<10	54 (58.1)	50 (56.8)	17 (58.6)	21 (72.4)	10 (47.6)	8 (42.1)
≥10	24 (25.8)	24 (27.3)	10 (34.5)	5 (17.2)	6 (28.6)	6 (31.6)
Unknown	15 (16.1)	14 (15.9)	2 (6.9)	3 (10.3)	5 (23.8)	5 (26.3)
PD-L1 combined positivity score, N (%)						
<10	37 (39.8)	36 (40.9)	14 (48.3)	12 (41.4)	5 (23.8)	5 (26.3)
≥10	25 (26.9)	22 (25.0)	6 (20.7)	9 (31.0)	9 (42.9)	7 (36.8)
Unknown	31 (33.3)	30 (34.1)	9 (31.0)	8 (27.6)	7 (33.3)	7 (36.8)

[A] For 7/74 patients with matched ctDNA and whole blood RNA, blood samples were obtained at different timepoints.

[B] In one patient the on-treatment RNA blood sample was collected after 8 weeks. This was before the third immunotherapy cycle, which was postponed. This patient is included in the 6 week group.

983